Supporting Information

PVP pre-intercalation engineering combined with V^{4+}/V^{5+} dual-valence modulation strategy for energy storage in aqueous zinc-ion batteries

Wenhui Mi,[a] Bosi Yin,[a] Haixi Gu,[a] Hanyu Wen,[a] Zhibiao Wang,[a] Hui Li,[b,c] Ziqian Yuan,[a] Siwen Zhang,*[a] and Tianyi Ma*[b,c]

Experimental Section

1. Sample preparation

Synthesis: Firstly, 4 mmol of V_2O_5 and 2 mmol of $Ca(OH)_2$ were added to 80 mL of deionized water. The aforementioned solution was then stirred at 70 °C for 3 hours. Subsequently, 100 mg of PVP was added to the yellow solution and stirred for an additional 30 minutes. Afterwards, the mixed solution was transferred into multiple 50 mL Teflon-lined stainless steel autoclave and held at 180 °C for 24 hours. Finally, the resultant products were washed several times with deionized water and ethanol. The obtained dark green product was dried in a vacuum oven at 60 °C for 12 hours, yielding PVP-doped PVP- CaVO nanorods. For comparison, CaVO was prepared by using the same procedure as the above mentioned without the introduction of PVP.

2. Electrochemical measurements

The electrochemical performances test of the electrodes are carried out by multi-channel electrochemical analyzer (VMP3, Bio-Logic-Science Instruments), NEWARE battery test system and CHI (760E, Chenhua), all experiments were performed at room temperature. Including cyclic voltammetry (CV), constant current charging and discharging (GCD), galvanostatic intermittent titration technique (GITT) and Electrochemical Impedance Spectroscopy (EIS) electrochemical workstation which is performed at an open circuit potential, and the perturbation from 10 kHz to 100 kHz is 5 mV.

3.Assembly of PVP-CaVO//Zn and CaVO//Zn of button cells

The PVP-CaVO//Zn button cell adopts the CR2032 model, where PVP-CaVO, Super P, and polyvinylidene fluoride (PVDF) are mixed in an N-methylpyrrolidone (NMP) solution in a ratio of 7:2:1 until a viscous slurry is formed. This slurry is then coated onto carbon paper and dried in a vacuum oven at 60 °C for 12 hours. Later, the cathode loading was around 1.2~1.5 mg cm^{-2}. The button cell is assembled with PVP-CaVO as the cathode, solid zinc as the anode, and 2M $Zn(CF_3SO_3)_2$ as the electrolyte. The manufacturing process for the PVP-CaVO//Zn button cell is similar to the one previously described, with the only difference being that the cathode utilizes CaVO instead of PVP-CaVO.

The energy density (E) and power density (P) of the devices were calculated using the following formula:

$$E = \int_0^t I V_{(t)} dt M \tag{1}$$

$$P = \frac{E}{t} \tag{2}$$

where I is the discharge current, t is the discharge time, dt is the time differential, $V_{(t)}$ is the discharge voltage at t, and M is the mass of active material.

4. Material characterization

To analyze the morphology of CaVO and PVP-CaVO cathodes, using a scanning electron microscope (SEM) equipped with an energy-dispersive X-ray spectroscopy (EDS) detector (SU8010; HITACHI). The morphological characteristics were further investigated through observations using a Transmission Electron Microscope (TEM) (JEOL 2100 F) and High-Resolution Transmission Electron Microscope (HRTEM) analysis. The crystal structures of were examined by X-ray diffraction (XRD) (Bruker D8-Advance). X-ray photoelectron spectroscopy (XPS) (ESCALAB 250Xi; Thermo Scientific Escalab) was used to clarify the surface elements and changes in valence state. The chemical structures are identified by FTIR (Thermo Scientific Nicolet iS20). The weight loss of materials was obtained by using thermo-gravimetric (TG) (Netzsch STA 449 F3) with a heating rate of 20 °C min^{-1} and air atmosphere.

Table S1. The comparison of capacity between this work and other previously reported literatures in aqueous zinc-ion batteries.

Cathode	Electrolyte	Current density ($A\ g^{-1}$)	Capacity ($mAh\ g^{-1}$)	Ref.
PVP-CaVO	2 M $Zn(CF_3SO_3)_2$	0.5 1 3 5 7 10	323.4 284.1 230.1 206.9 197.6 181.1	This work
D-MoS_2-O	3 M $Zn(CF_3SO_3)_2$	0.5 1 3 5 8 10	228.2 203.8 153.3 134.1 111.6 102.4	1
$Na_5V_{12}O_{32}$	2M $ZnSO_4$	0.5 1 2 5	244.5 199.0 121.3 59.7	2
$HNaV_6O_{16}\cdot 4H_2O$	2M $ZnSO_4$	0.5 1 2 5	295.4 207.6 140.6 77.8	2
$Vo^{\cdot\cdot}$-PNVO	3 M $Zn(CF_3SO_3)_2$	0.4 0.8 1 2 4	228.0 224.0 221.0 205.0 165.0	3
PA-VOP	2M $Zn(CF_3SO_3)_2$	0.5 1 2 5	254.8 236.4 220.7 207.2	4
$H_2V_3O_8$	3 M $Zn(CF_3SO_3)_2$	0.5 1 3 5	297.4 240.5 155.0 113.9	5

$Na_2V_6O_{16}\cdot 1.63H_2O$	3 M $Zn(CF_3SO_3)_2$	0.5	261.0	6
		1	219.0	
		2	162.0	

Fig. S1. Macroscopic photographs of the CaVO and PVP-CaVO.

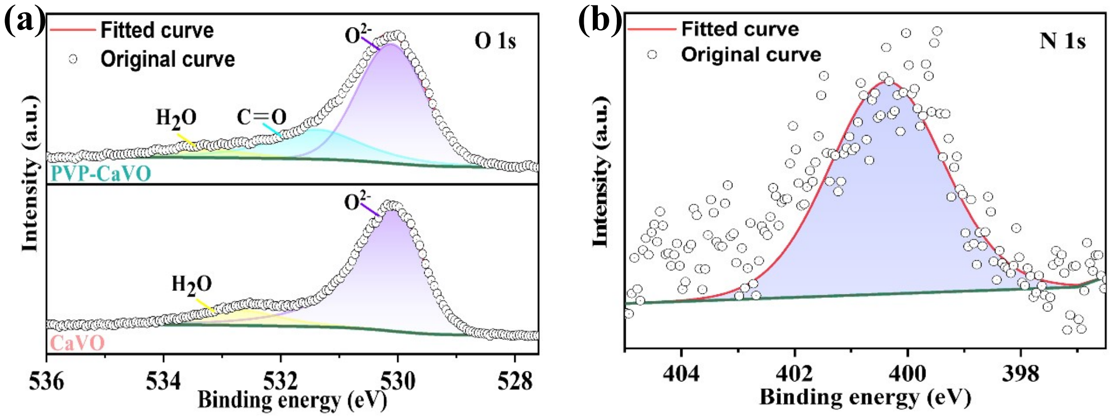

Fig. S2. (a) High-resolution XPS O 1s spectra of PVP-CaVO and CaVO, (b) N 1s spectra of PVP-CaVO.

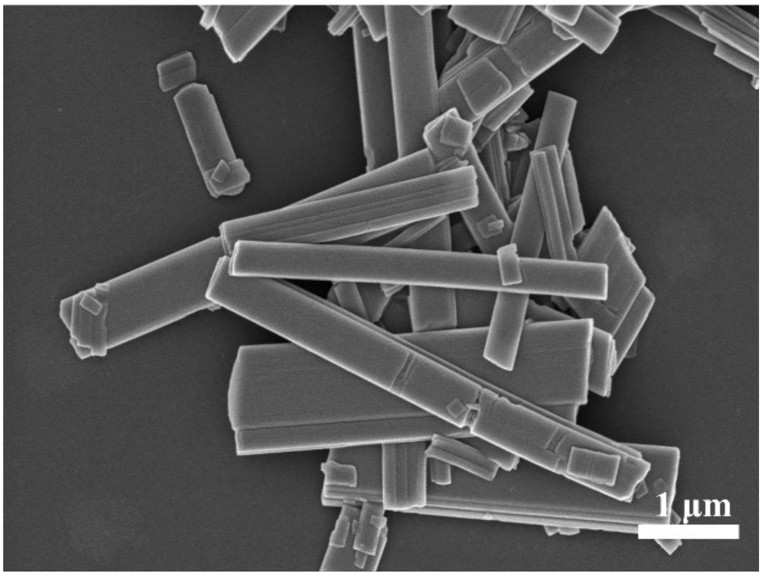

Fig. S3. SEM image of the CaVO.

Fig. S4. TEM image of the CaVO.

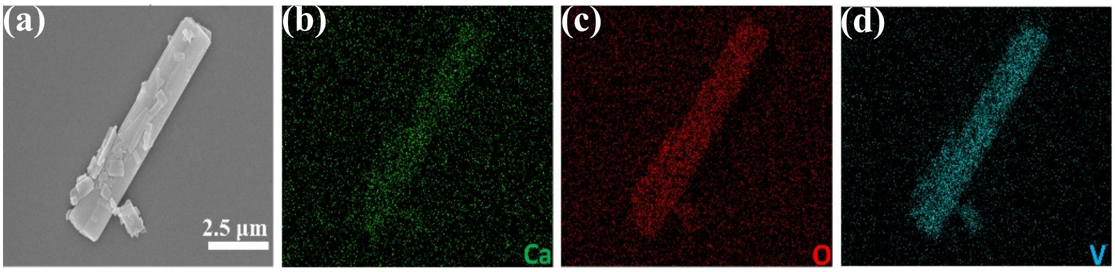

Fig. S5. (a-d) The elemental mapping images of the CaVO.

Map Sum Spectrum				
Element	Line Type	Weight %	Weight % Sigma	Atomic %
C	K series	21.15	0.71	31.07
N	K series	3.38	1.58	4.26
O	K series	50.75	1.08	55.96
Ca	K series	1.55	0.14	0.68
V	K series	23.17	0.55	8.02
Total		100.00		100.00

Map Sum Spectrum				
Element	Line Type	Weight %	Weight % Sigma	Atomic %
O	K series	73.84	0.55	89.72
Ca	K series	2.86	0.26	1.39
V	K series	23.30	0.50	8.89
Total		100.00		100.00

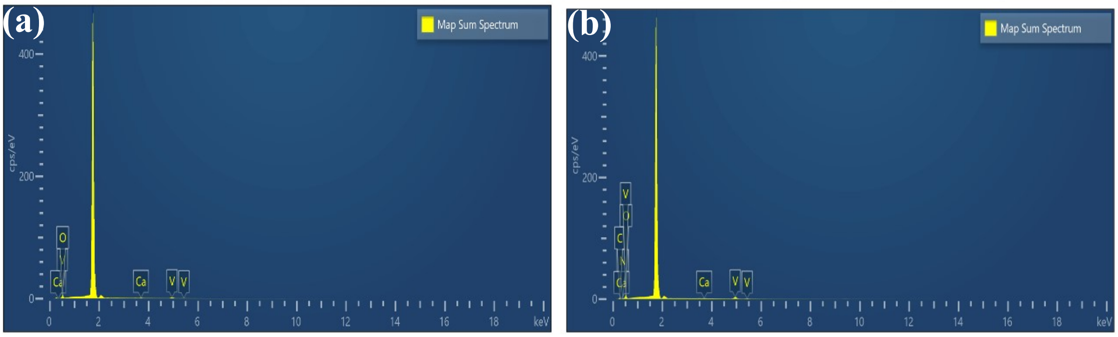

Fig. S6. (a-b) EDS images of the PVP-CaVO and CaVO.

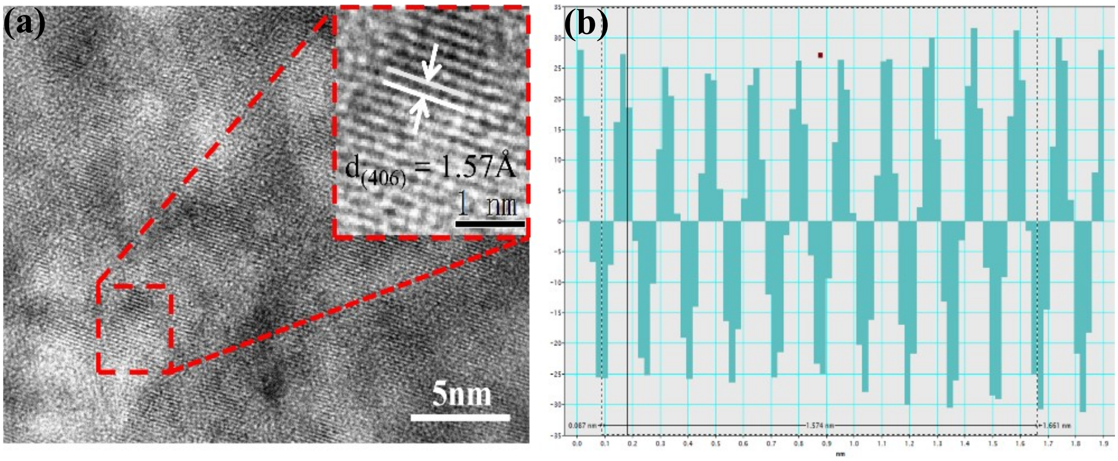

Fig. S7. (a-b) TEM image of the CaVO.

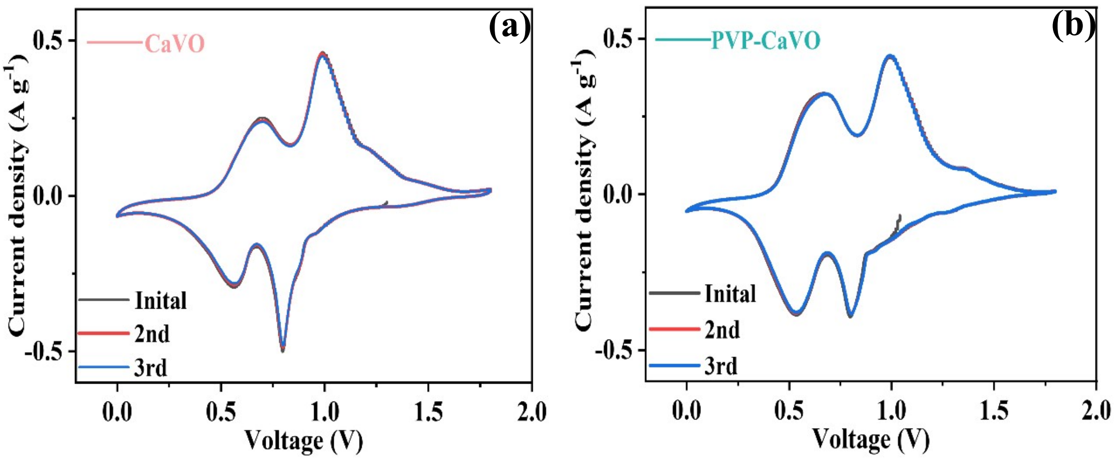

Fig. S8. (a-b) CV curves of the CaVO and PVP-CaVO at 0.2 mV s^{-1}.

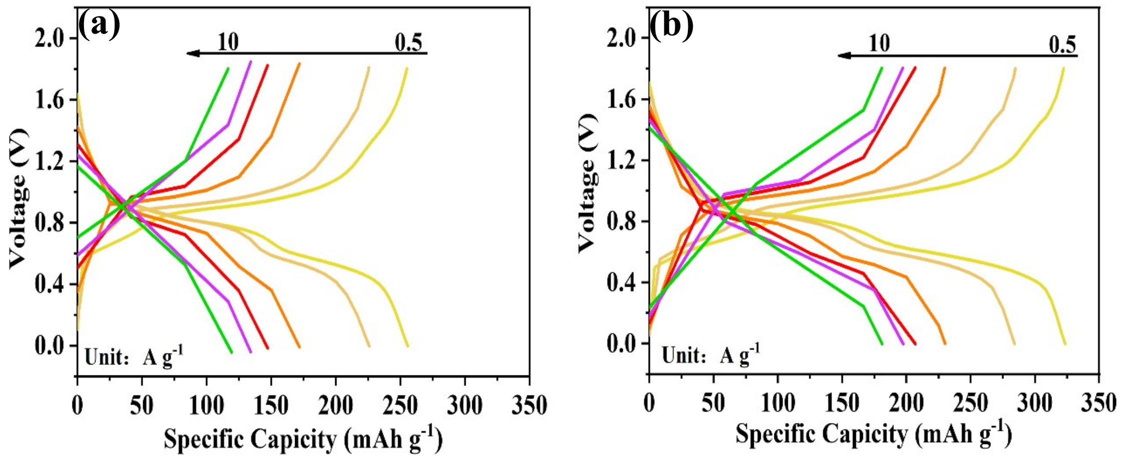

Fig. S9. (a-b) GCD curves of the PVP-CaVO and CaVO at 0.5 A g^{-1}, 1.0 A g^{-1}, 3.0 A g^{-1}, 5.0 A g^{-1}, 7.0 A g^{-1} and 10.0 A g^{-1}.

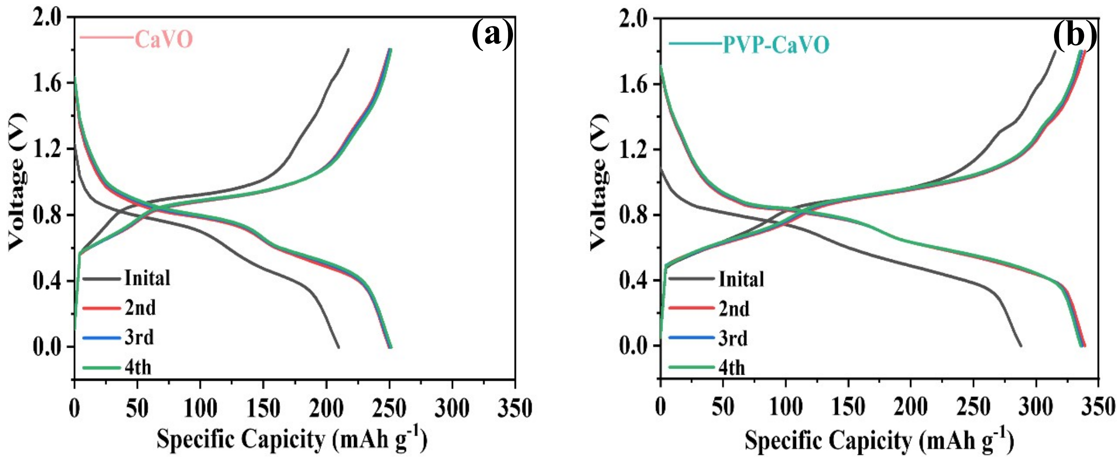

Fig. S10. (a-b) The GCD curves of CaVO and PVP-CaVO at a scan rate of 0.5 A g^{-1}.

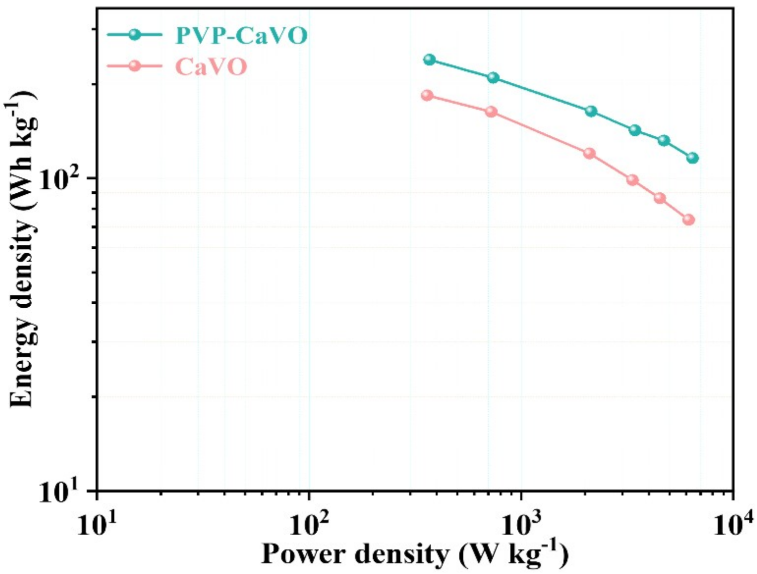

Fig. S11. Ragone plots of CaVO and PVP-CaVO.

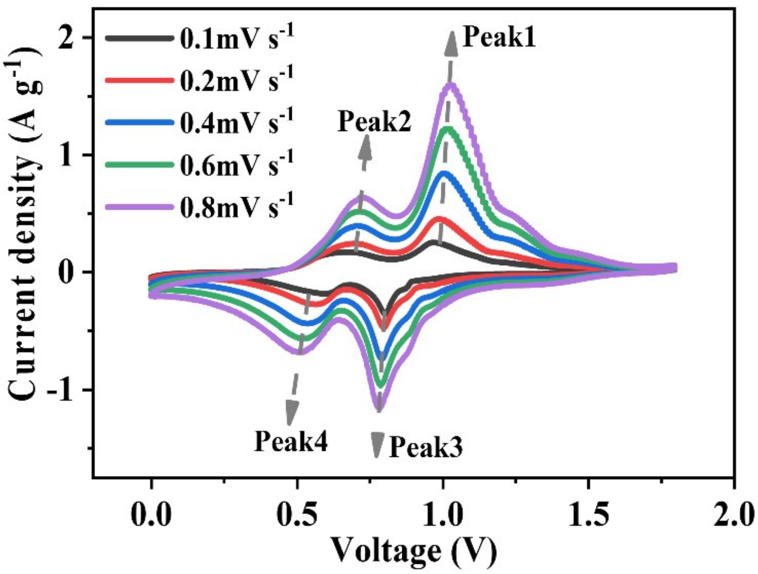

Fig. S12. The CV curves of CaVO at different scan rates.

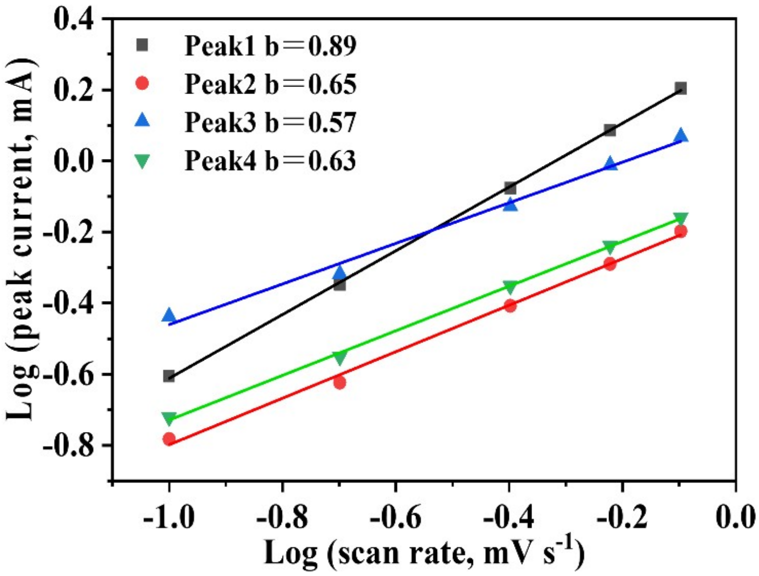

Fig. S13. The corresponding plots of log (peak current) vs. log (scan rate) at each peak.

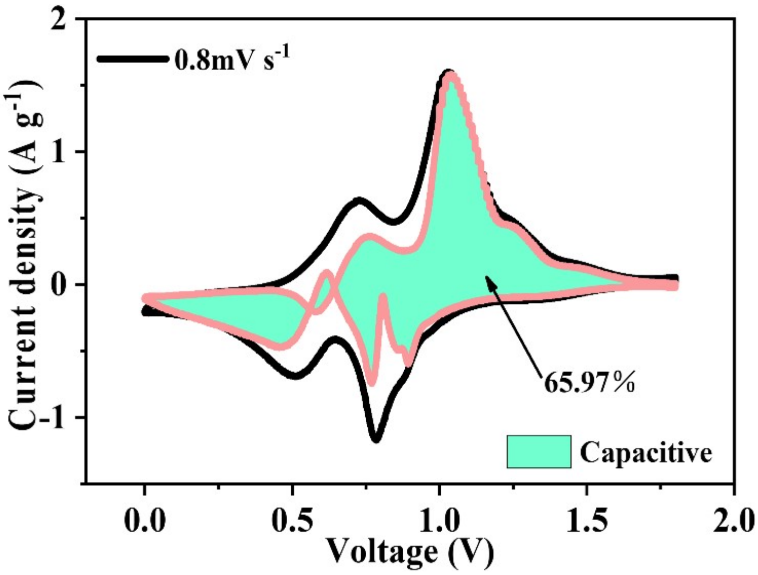

Fig. S14. Capacitive contributions to the total current for CaVO at 0.8mV s-

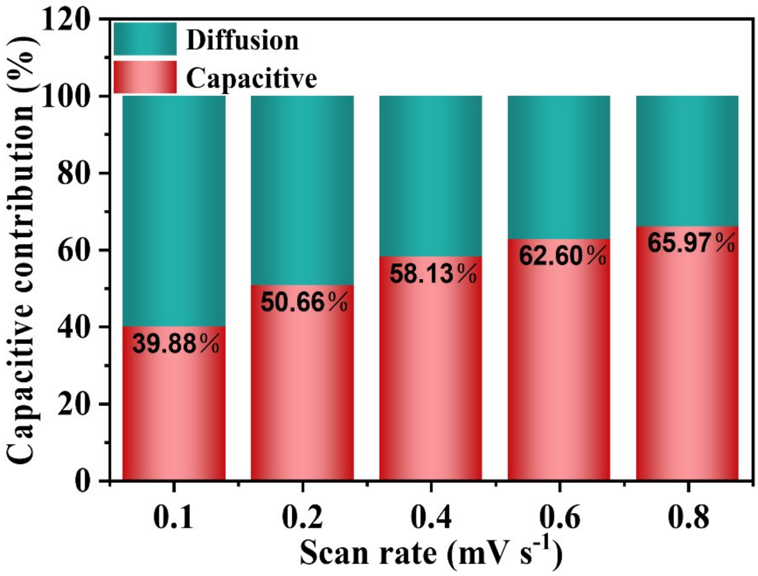

Fig. S15. The capacitive contributions of CaVO at different scan rates.

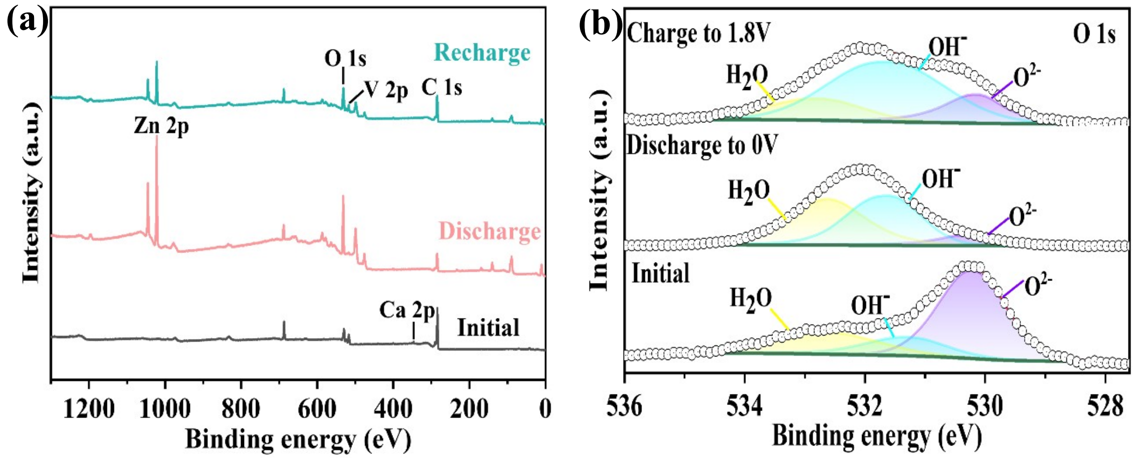

Fig. S16. (a-b) High-resolution XPS spectra of survey spectra and O 1s.

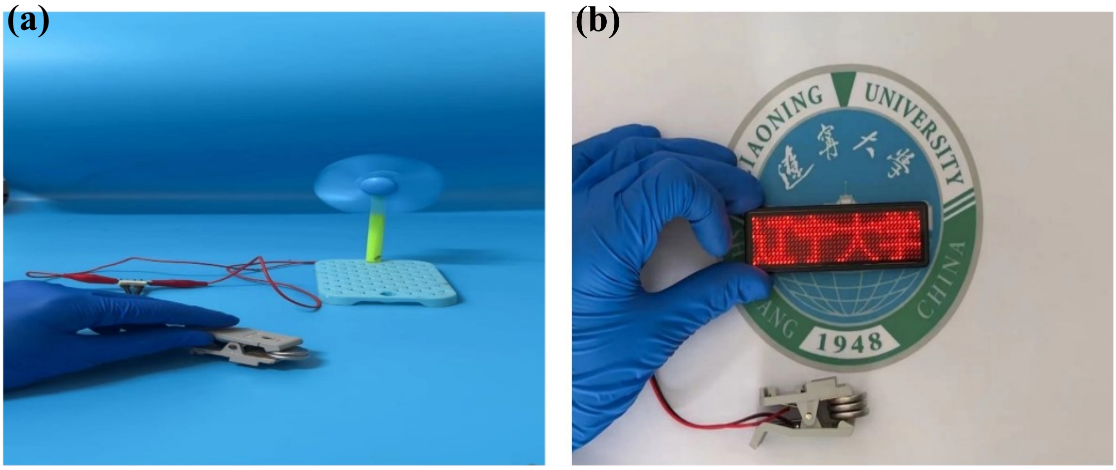

Fig. S17. (a-b) Photographs of powering a fan and an LED ligh

Reference

1 S. Li, Y. Liu, X. Zhao, K. Cui, Q. Shen, P. Li, X. Qu and L. Jiao, *Angew. Chem. Int. Ed.*, 2021, **60**, 20286-20293.

2 X. Guo, G. Fang, W. Zhang, J. Zhou, L. Shan, L. Wang, C. Wang, T. Lin, Y. Tang and S. Liang, *Adv. Energy Mater.*, 2018, **8**, 1801819.

3 W. Bi, G. Gao, G. Wu, M. Atif, M. S. AlSalhi and G. Cao, *Energy Storage Mater.*, 2021, **40**, 209-218.

4 L. Hu, Z. Wu, C. Lu, F. Ye, Q. Liu and Z. Sun, *Energy Environ. Sci.*, 2021, **14**, 4095-4106.

5 P. He, Y. Quan, X. Xu, M. Yan, W. Yang, Q. An, L. He and L. Mai, *Small*, 2017, **13**, 1702551.

6 P. Hu, T. Zhu, X. Wang, X. Wei, M. Yan, J. Li, W. Luo, W. Yang, W. Zhang, L. Zhou, Z. Zhou and L. Mai, *Nano Lett.*, 2018, **18**, 1758-1763.